Journal of
Water & Climate Change

IWA PUBLISHING

Journal of Water and Climate Change Vol 13 No 9, 3435 doi: 10.2166/wcc.2022.180

Multivariate analysis of multiscale periodicity in North American annual mean sea level based on wavelet coherence and multiple wavelet coherence

Chao Song[a,b,c] and Xiaohong Chen[a,b,c,*]

[a] Center for Water Resources and Environment, School of Civil Engineering, Sun Yat-sen University, Guangzhou 510275, China
[b] Guangdong Engineering Technology Research Center of Water Security Regulation and Control for Southern China, School of Civil Engineering, Sun Yat-sen University, Guangzhou 510275, China
[c] Key Laboratory of Water Cycle and Water Security in Southern China of Guangdong High Education Institute, School of Civil Engineering, Sun Yat-sen University, Guangzhou 510275, China
*Corresponding author. E-mail: eescxh@mail.sysu.edu.cn

ABSTRACT

The relationships between sea levels and single climate indexes have been widely explored. However, sea level is controlled by multiple climate factors simultaneously with differences among places and time scales. Despite this, few studies have addressed the relationships between sea levels and multiple climate indexes. Here, the interrelations between the annual mean sea level (AMSL) and individual climate indexes and combinations of climate indexes were characterized by wavelet coherence (WTC) and multiple wavelet coherence (MWC). The results showed that six climate indexes had a significant correlation with AMSL, among which the Atlantic Multidecadal Oscillation (AMO) had the least significant correlation, but Niño3.4 had the significant correlation. The average significant coherence area (PASC) value for Niño3.4 was 14.03% and its average wavelet coherence (AWC) value was 0.79. By combining climate indexes, the average values of PASC and AWC can be significantly increased. The average PASC and AWC values of the five climate index combinations were the largest, 95.87% and 0.965, respectively, followed by four, three, and two index combinations. A single climate index is not sufficient to explain sea level change in North America. Sea level changes in North America require between three and five climate indexes to explain, depending on the region. By calculating PASC and AWC values, this study provides the possibility to understand the impact of the combined effects of multiple climate indexes on AMSL, is of great help to screen the best predictor of sea level, and provides a new method to reveal the complex mechanism of sea level change.

Key words: annual mean sea level, combined effects, multiple wavelet coherence, North America, optimal climate index combination, wavelet coherence

HIGHLIGHTS

- Multiple wavelet coherence is first used to study the relationship between the annual mean sea level and multiple climate indexes.
- We determine the optimal climate index combination for the annual mean sea level in North America.
- We analyze the multiple time scales and dominant periods of the annual mean sea level in North America.

1. INTRODUCTION

Sea level is an important indicator of climate change and it changes along broad spatial and temporal scales. To reveal the physical mechanisms underlying sea level change it is necessary to study the relationship between sea level and climate indices on temporal and spatial scales. To date, research on sea level has mostly focused on the estimation of regional and global sea level rise (Hannah & Bell 2012; Wenzel & Schröter 2014; Hamlington & Thompson 2015) and the influence of atmospheric circulation on sea level change (Chafik *et al.* 2019). There are significant interannual and interdecadal variabilities in sea level, and these variations exhibit the characteristics of multiple periodic signals. Therefore, selecting analytical methods that have a robust periodic analysis ability is crucial to the study of sea level change.

The wavelet coherence (WTC) method is a robust tool for analyzing the physical mechanisms underlying periodic signals. This method was initially proposed to analyze the El Niño-Southern Oscillation (ENSO) time series. Later, Grinsted *et al.* (2004) applied it to geophysical time series, further demonstrating its capability to analyze the physical mechanisms

underlying periodic variability. It has since been widely promoted and applied in various fields. For example, runoff (Tang *et al.* 2018; Wang *et al.* 2018) and lake level (Nourani *et al.* 2019). Over time the cross-wavelet has been greatly developed and used to analyze periodic cycles caused by a variety of physical mechanisms. These have included precipitation and groundwater (Yu & Lin 2015), runoff and climate indexes (Durocher *et al.* 2016), global mean temperature anomalies and sea level (Kirikkaleli & Sowah 2021), Baltic Sea level and zonal wind (Medvedev & Kulikov 2019), Pacific Decadal Oscillation (PDO) and sea level in the South China Sea (Xi *et al.* 2020), positive pressure sea level over the tropical Indian Ocean basin and the northern winter Madden-Julian oscillation (Rohith *et al.* 2019), Atlantic meridional overturning circulation and Mediterranean Sea level (Volkov *et al.* 2019), ocean signal and sea level change (Jevrejeva *et al.* 2006), ENSO and the Baltic Sea (Jevrejeva *et al.* 2003), sea level response of the Indian Ocean and ENSO (Tiwari *et al.* 2004), and East China Sea level and ENSO events (Liu *et al.* 2010). Recently, Piecuch *et al.* (2019) used the cross-wavelet to reveal the internal relationship between sea level off the New England coast and the Atlantic meridional overturning circulation at 26 °N. Little *et al.* (2021) used cross wavelets to reveal the high power and space–time complexity of the sea level along the east coast of North America on an interdecadal time scale. It can be seen that the cross-wavelet has become prevalent in the analysis of periodic oceanic signals.

WTC can only reflect the relationship between the two variables on the time scale. Previous studies have shown that a single climate index is not sufficient to explain sea level change (Little *et al.* 2021). In addition, sea level change can be influenced by multiple climate indexes and their interactions simultaneously. Therefore, if we only include a single factor in the analysis, it will be unable to fully characterize the observed changes. However, the disadvantage of existing multivariate methods is that they cannot reflect this relationship on a time scale, multivariate wavelet coherence (MWC) can determine the multivariate relationship between prediction variables and response variables on the time scale. Here, to overcome the shortcomings of wavelet coherence (WTC) and existing multivariate methods, and try to reveal the combined effects of multiple climate indexes on AMSL, we introduced the MWC invented by Hu & Si (2016). For the application of MWC, Gu *et al.* (2021) used it to evaluate the multivariate relationship of a local groundwater system, Song *et al.* (2020) used it to explore the potential relationship between extreme precipitation and a large-scale climate model, Nalley *et al.* (2019) used it to examine the multiscale relationship between precipitation, runoff change, ENSO, North Atlantic Oscillation (NAO), and PDO, and Cheng *et al.* (2021) used it to determine the relationship between base flow and meteorological factors/large-scale circulation indexes.

Nevertheless, there is still something worth exploring in this field of study. (1) Although cross wavelets have been used to analyze sea level until now no scholars have used MWC to study the relationship between AMSL and multiple climate indexes. (2) We used MWC to determine which four climate indexes are the best combination of the four climate indexes. (3) We determined how many climate indexes are adequate to explain AMSL in North America.

This paper is organized as follows: The principles of the WTC and MWC are introduced in Section 2. The study area and data sources are presented in Section 3. Section 4 relates the results of the WTC and MWC analyses. The discussion section is presented in Section 5. Conclusions are drawn in Section 6.

2. MATERIALS AND METHODS

2.1. Study area

We selected 82 stations along the coast of North America as the study area, the longest sequence was 166 years and the shortest was 31 years. The sequence lengths and AMSL change trends of the 82 stations are shown in Figure 1. The longitude, latitude, name, and other related information of each station are shown in Table 1. For more information on the data, please refer to Holgate *et al.* (2013) and PSMSL (2021).

2.2. Data sources

According to the research of Zhang & Church (2012), ENSO and PDO can explain 60% of the total sea level change in the era of elevation measurements, so ENSO and PDO are strong influences on the change in AMSL. ENSO indexes use time series of area-averaged SST (e.g., Niño3.4: from 5 °N to 5 °S and from 170 °W to 120 °W) to identify El Niño and La Niña events. The PDO index was identified as the leading principal component of the variability of the North Pacific (poleward of 20 °N) monthly sea surface temperature (SST) (Mantua *et al.* 1997). Therefore, in this study, we selected the Niño3.4 and PDO indexes. The NAO determines climate change from the East coast of the United States to Siberia, and from the Arctic to the subtropical Atlantic (Hurrell *et al.* 2003). The Southern Oscillation Index (SOI) is the difference in sea level

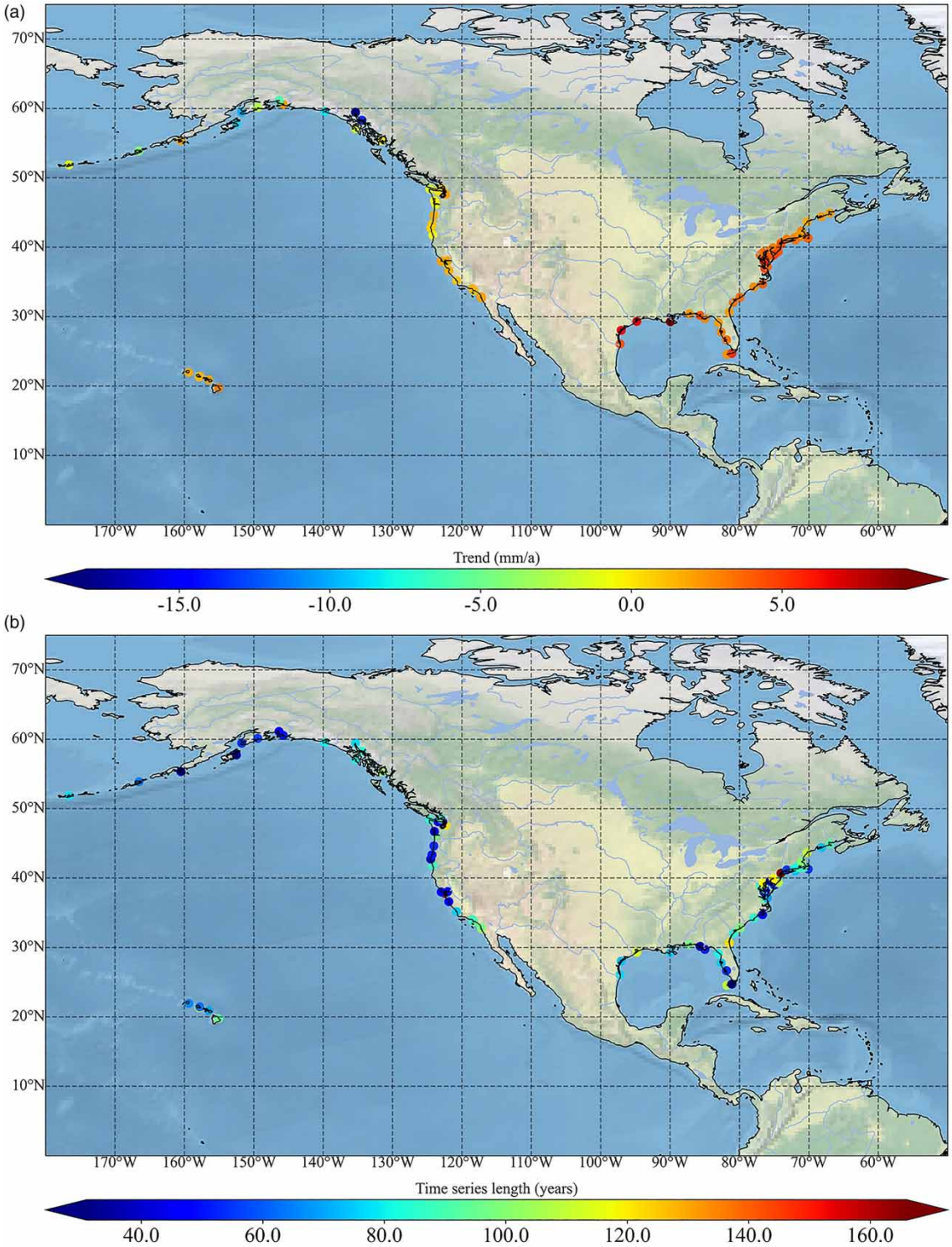

Figure 1 | Change trends (a) and sequence lengths (b) of AMSL at 82 stations. (It is worth noting that the circles in the figure represent stations, for which detailed location information is shown in Table 1.)

pressure between Tahiti (148 °05′W, 17 °53′S) or Easter Island (109 °30′W, 29 °00′S) and Darwin (125 °59′E, 12 °20′S). A negative SOI corresponds to an El Niño event, while a positive SOI corresponds to a La Niña event. The Atlantic Multidecadal Oscillation (AMO) index refers to the annual mean of SST anomalies in the region from 75 °W to 7.5 °W and 0 °N to 60 °N. The

Table 1 | Latitude and longitude information for 82 stations

Station	Station number	Latitude	Longitude	Station	Station number	Latitude	Longitude
SAN FRANCISCO	10	37.807	−122.465	YAKUTAT	445	59.548	−139.733
NEW YORK (THE BATTERY)	12	40.7	−74.013	ADAK SWEEPER COVE	487	51.863	−176.632
FERNANDINA BEACH	112	30.672	−81.465	SKAGWAY	495	59.45	−135.327
SEATTLE	127	47.602	−122.338	PORT ISABEL	497	26.06	−97.215
PHILADELPHIA (PIER 9N)	135	39.933	−75.142	PORT SAN LUIS	508	35.177	−120.76
BALTIMORE	148	39.267	−76.578	ST. PETERSBURG	520	27.76	−82.627
HONOLULU	155	21.307	−157.867	GRAND ISLE	526	29.263	−89.957
SAN DIEGO (QUARANTINE STATION)	158	32.713	−117.173	MONTAUK	519	41.048	−71.96
GALVESTON II, PIER 21, TX	161	29.31	−94.793	BAR HARBOR, FRENCHMAN BAY, ME	525	44.392	−68.205
ATLANTIC CITY	180	39.355	−74.418	ROCKPORT	538	28.022	−97.047
PORTLAND (MAINE)	183	43.657	−70.247	KAHULUI HARBOR, MAUI ISLAND	521	20.895	−156.477
KEY WEST	188	24.555	−81.807	KIPTOPEKE BEACH	636	37.165	−75.988
LEWES (BREAKWATER HARBOR)	224	38.782	−75.12	NAWILIWILI BAY, KAUAI ISLAND	756	21.953	−159.355
KETCHIKAN	225	55.332	−131.625	UNALASKA	757	53.88	−166.537
BOSTON	235	42.353	−71.053	MOKUOLOE ISLAND	823	21.432	−157.79
CHARLESTON I	234	32.782	−79.925	SEWARD	266	60.12	−149.427
LOS ANGELES	245	33.72	−118.272	BRIDGEPORT	1068	41.173	−73.182
PENSACOLA	246	30.403	−87.21	NANTUCKET ISLAND	1111	41.285	−70.097
LA JOLLA (SCRIPPS PIER)	256	32.867	−117.257	SELDOVIA	1070	59.44	−151.72
ASTORIA (TONGUE POINT), OR	265	46.207	−123.768	FORT MYERS	1106	26.647	−81.87
HILO, HAWAII ISLAND	300	19.73	−155.055	CAPE MAY	1153	38.968	−74.96
SEWELLS POINT, HAMPTON ROADS	299	36.947	−76.33	SOUTH BEACH	1196	44.625	−124.042
ANNAPOLIS (NAVAL ACADEMY)	311	38.983	−76.48	APALACHICOLA	1193	29.727	−84.982
EASTPORT	332	44.903	−66.982	CORDOVA	566	60.558	−145.752
NEWPORT	351	41.505	−71.327	CHARLESTON II	1269	43.345	−124.322
WASHINGTON DC	360	38.873	−77.022	CAMBRIDGE II	1295	38.573	−76.068
SANDY HOOK	366	40.467	−74.008	LEWISETTA, VA	2324	37.995	−76.465
WOODS HOLE (OCEAN. INST.)	367	41.523	−70.672	PORT TOWNSEND	1325	48.112	−122.757
SANTA MONICA (MUNICIPAL PIER)	377	34.008	−118.5	BEAUFORT, NC	2295	34.72	−76.67
CRESCENT CITY	378	41.745	−124.182	MONTEREY	1352	36.605	−121.887
FRIDAY HARBOR (OCEAN. LABS.)	384	48.547	−123.01	VALDEZ	1353	61.125	−146.362
NEAH BAY	385	48.367	−124.612	POINT REYES	1394	37.995	−122.977
FORT PULASKI	395	32.033	−80.902	PORT ANGELES, WA	2127	48.125	−123.44
WILMINGTON	396	34.227	−77.953	PORT CHICAGO, CA	2330	38.055	−122.04

(*Continued.*)

Table 1 | Continued

Station	Station number	Latitude	Longitude	Station	Station number	Latitude	Longitude
JUNEAU	405	58.298	−134.412	TOKE POINT, WILLIPA BAY, WA	1354	46.707	−123.967
SOLOMON'S ISLAND (BIOL. LAB.)	412	38.317	−76.452	KODIAK ISLAND, WOMENS BAY	567	57.732	−152.512
SITKA	426	57.052	−135.342	SAND POINT, POPOF IS., AK	1634	55.337	−160.502
CEDAR KEY II	428	29.135	−83.032	PORT ORFORD	1640	42.738	−124.498
NEW LONDON	429	41.36	−72.09	PANAMA CITY, ST.ANDREWS BAY, FL	1641	30.152	−85.667
PROVIDENCE (STATE PIER)	430	41.807	−71.4	REEDY POINT	786	39.558	−75.573
ALAMEDA (NAVAL AIR STATION)	437	37.772	−122.298	VACA KEY	1701	24.712	−81.105

tripole index (TPI) is based on the difference between the sea surface temperature anomalies (SSTAs) averaged over the central equatorial Pacific and the average of the SSTA in the Northwest and Southwest Pacific (Henley *et al.* 2015).

The annual mean sea level (AMSL) data for North America were obtained from the Permanent Service for Mean Sea Level (https://www.psmsl.org/data/obtaining/complete.php). The NAO, Niño3.4 index, AMO, and SOI were provided by NOAA/ESRL (data source: https://www.esrl.noaa.gov/psd/gcos_wgsp/Timeseries/). The PDO was acquired from the NOAA National Centers for Environmental Information (https://www.ncdc.noaa.gov/teleconnections/PDO/). The TPI was acquired from the NOAA Physical Sciences Laboratory (https://psl.noaa.gov/data/timeseries/IPOTPI/tpi.timeseries.ersstv5.data). For annual climate data, we took the average of each of the four seasons: spring, summer, autumn, and winter.

2.3. Methods

2.3.1. Wavelet coherence

The advantage of wavelet coherence in the hydrological application is that it reveals the coherence of prediction variables and response variables in the time and frequency domain. We define the WTC of two time series as (Grinsted *et al.* 2004):

$$R_n^2(s) = \frac{|S(s^{-1}W_n^{XY}(s))|^2}{S(s^{-1}|W_n^X(s)|^2) * S(s^{-1}|W_n^Y(s)|^2)} \tag{1}$$

where S is a smoothing operator; and $W_n^X(s)$ is the continuous wavelet transform of X series. Note that this definition closely resembles that of a traditional correlation coefficient, and it is useful to think of the wavelet coherence as a correlation coefficient localized in time frequency space. We write the smoothing operator S as:

$$S(W) = S_{scale}(S_{time}(W_n(s))) \tag{2}$$

where S_{scale} is smoothing along the wavelet scale axis; and S_{time} is smoothing in time. For the Morlet wavelet, a suitable smoothing operator was proposed by Torrence & Webster (1999):

$$S_{time}(W)|_s = (W_n(s) * c_1^{(-t^2/2s^2)})|_s, \quad S_{time}(W)|_n = (W_n(s) * c_2 \Pi(0.6s))|_n \tag{3}$$

where c_1 and c_2 are normalization constants and Π is the rectangle function. The factor of 0.6 is the empirically determined scale decorrelation length for the Morlet wavelet (Torrence & Compo 1998).

It should be noted that we evaluate the performances of single factors and combined factors using the average wavelet coherence (AWC, the average of the coherence value in the significant coherence region) and the percentage of significant coherence area (PASC, 100 * significant coherence area/(significant coherence area + insignificant coherence area)). The larger the PASC, the more important that single factor or combination of factors is, the same applies to MWC. It should

be noted that a larger PASC tends to correspond to a larger AWC, and smaller PASC values do not correspond to larger AWC values. However, whether the variable is the dominant variable should be reflected by PASC value.

2.3.2. Multiple wavelet coherence

WTC can be thought of as the traditional correlation coefficient localized in the scale-location domain (Grinsted *et al.* 2004). The wavelet correlation coefficient can be extended from two variables to multiple variables (>2) and, in the same way, the wavelet coherence between two variables can be extended to multiple variables. Similar to bivariate wavelet coherence, MWC utilizes a series of auto- and cross-wavelet power spectra at different scales and spatial (or temporal) locations for the response variable and all predictor variables (Hu & Si 2016).

A matrix representation of the smoothed auto- and cross-wavelet power spectra for multiple predictor variables $X(X = \{X_1, X_2, \ldots, X_q\})$ is defined as below (Hu & Si 2016):

$$\overleftrightarrow{W}_{X,X}(s,\tau) = \begin{bmatrix} \overleftrightarrow{W}^{X_1,X_1}(s,\tau) & \overleftrightarrow{W}^{X_1,X_2}(s,\tau) & \ldots & \overleftrightarrow{W}^{X_1,X_q}(s,\tau) \\ \overleftrightarrow{W}^{X_2,X_1}(s,\tau) & \overleftrightarrow{W}^{X_2,X_2}(s,\tau) & \ldots & \overleftrightarrow{W}^{X_2,X_q}(s,\tau) \\ \vdots & \vdots & & \vdots \\ \overleftrightarrow{W}^{X_q,X_1}(s,\tau) & \overleftrightarrow{W}^{X_q,X_2}(s,\tau) & \ldots & \overleftrightarrow{W}^{X_q,X_q}(s,\tau) \end{bmatrix} \tag{4}$$

where $\overleftrightarrow{W}^{X_i,X_j}(s,\tau)$ is the smoothed auto-wavelet power spectra (when $i = j$) or cross-wavelet power spectra (when $i \neq j$) at scale s and spatial (or temporal) location τ, respectively (Hu & Si 2016).

The matrix of the smoothed cross-wavelet power spectra between the response variable Y and multiple predictor variables X can be defined as:

$$\overleftrightarrow{W}^{Y,X}(s,\tau) = [\overleftrightarrow{W}^{Y,X_1}(s,\tau) \quad \overleftrightarrow{W}^{Y,X_2}(s,\tau) \quad \ldots \overleftrightarrow{W}^{Y,X_q}(s,\tau)] \tag{5}$$

where $\overleftrightarrow{W}^{Y,X_i}(s,\tau)$ is the cross-wavelet power spectra (when $i \neq j$) between Y and X_i at scale s and spatial (or temporal) location τ (Hu & Si 2016).

The MWC at scale s and location τ, $\rho_m^2(s,\tau)$ can be written as:

$$\rho_m^2(s,\tau) = (\overleftrightarrow{W}^{Y,X}(s,\tau)\overleftrightarrow{W}^{X,X}(s,\tau)^{-1}\overline{\overleftrightarrow{W}^{Y,X}(s,\tau)})/(\overleftrightarrow{W}^{Y,Y}(s,\tau) \tag{6}$$

where $\overline{\overleftrightarrow{W}^{Y,X}(s,\tau)}$ is a complex conjugate of $(\overleftrightarrow{W}^{Y,X}(s,\tau)$.

3. RESULTS

3.1. Results of WTC analysis

We use WTC to analyze the relationship between AMSL and a single climate index on a time scale. The relationship between Niño3.4 and AMSL on a time scale is shown in Figure 2.

We found that AMSL of most stations has significant correlation with Niño3.4 over a period of 4–8 years, which corresponds to the quasi period of ENSO. The coherence between Niño3.4 and AMSL was complex. Some stations had large areas of significant coherence between AMSL and Niño3.4, such as stations 1196–1634, 300–385, 636–823, 537, 508, and 1196–1634. The years when stations exhibited significant coherence generally corresponded to either EI Niño events (i.e., 1939–1941, 1965–1966, 1972–1976, 1982, 1997–1998, 2006–2007, 2009, and 2010) or La Niña events (i.e., 1970, 1984, 1988–1989, 1998–2001, 2007–2008, and 2010–2011) (Haddad *et al.* 2013). Furthermore, at some stations the AMSL did not have any significant coherence with Niño3.4 (i.e., stations 112, 183, 188, 234, 1641, and 430).

In general, the effects of Niño3.4 on sea level changes in North America appeared localized. The significant coherence between PDO and AMSL is shown in Figure 3.

The coherences between AMSL and PDO were complex. Not all stations had relatively large PASC values (PASC value was above 15%), and some stations even had relatively small (PASC value was less than 15%). For example, the PASC values at stations 12, 112, 161, 224, 246, 351, 360, 395, 396, 299, 311, 332, 1106, 430, 497, and 636 (longitudes ranging

Figure 2 | Wavelet coherence between AMSL and Niño3.4. (Thick contours denote 5% significance levels against red noise, the areas outside the cones represent the areas where edge effects might distort the results, which is an invalid area. The arrow denotes the relative phase relationships (positive correlation, arrows point right; negative correlation, arrows point left). The color denotes the strength of coherence.) Please refer to the online version of this paper to see this figure in colour: http://dx.doi.org/10.2166/wcc.2022.180.

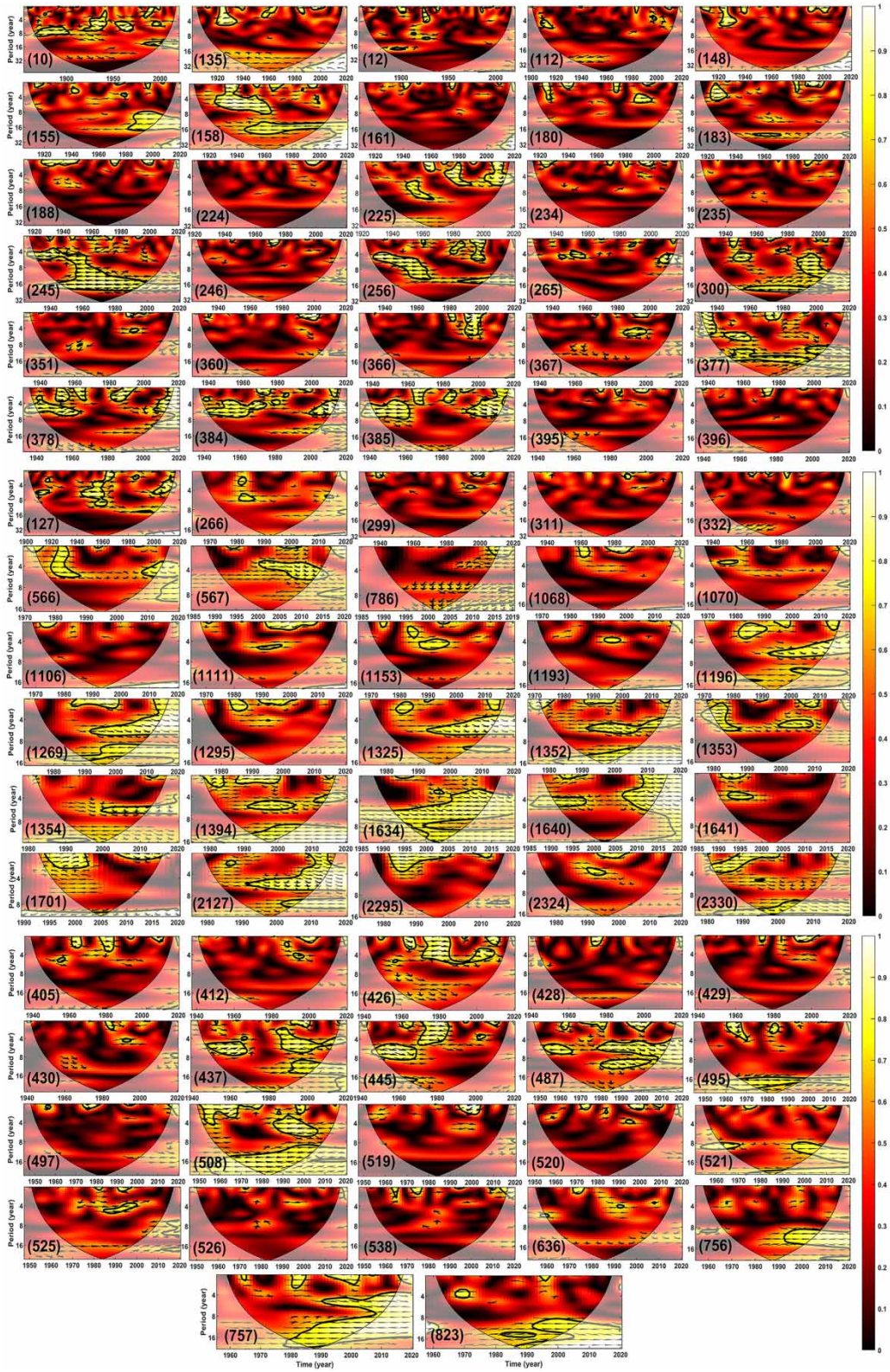

Figure 3 | Wavelet coherence between AMSL and PDO. (Thick contours denote 5% significance levels against red noise, the areas outside the cones represent the areas where edge effects might distort the results, which is an invalid area. The arrow denotes the relative phase relationships (positive correlation, arrows point right; negative correlation, arrows point left). The color denotes the strength of coherence.) Please refer to the online version of this paper to see this figure in colour: http://dx.doi.org/10.2166/wcc.2022.180.

from about 70 °W to 95 °W) were relatively small, indicating that PDO had a relatively small effect on the changes in AMSL at these stations. In addition, the PASC of AMSL and PDO at stations 158, 245, 256, 300, 377, 378, 384, 385, 566, 567, 1269, 1325, 1352, 1394, 1634, 1640, 2127, 487, 508, and 757 (ranging approximately from 120 °W to 125 °W) were relatively large, which meant that PDO had a greater influence on the changes in AMSL at these stations. For the stations with larger PASC, we found that the time periods of PDO coherence to AMSL were generally between 4–8 years and 8–16 years, and this periodicity also lasted for a long time. The effects of PDO on sea level changes in North America also appeared localized.

Due to the length and structure of the manuscript, we do not provide details on the significant coherence between AMSL and SOI, NAO, AMO, or TPI. However, we do summarize the results of PASC and AWC for the 82 stations under the six climate indexes in Figures 4 and 5, respectively.

There were significant differences between the PASC of the six climate indicators for AMSL. The average PASC values of Niño3.4, PDO, TPI, SOI, NAO, and AMO were 14.03, 9.86, 12.92, 10.86, 8.80, and 6.07%, respectively. The average PASC values of Niño3.4, TPI, and SOI were relatively large, while those of NAO and AMO were lower. Niño3.4 had the highest PASC average. This meant that the average influences of NAO and AMO on AMSL were lower than that of Niño3.4, PDO, TPI, and SOI on AMSL. Among the six climate indexes, Niño3.4 had the largest average impact on AMSL, followed by TPI, SOI, PDO, NAO, and AMO, in that order. In addition, the average PASC of Niño3.4, PDO, SOI, and TPI within the 115°–125 °W range was greater than that of the 65°–90 °W range, which meant that the impacts of these indexes on AMSL were greater at 115°–125 °W than at 65°–90 °W.

The differences between the AWC of AMSL for the six climate indexes were not very large, which was also true for the AWC of the different stations. The coherence range (the largest of the 82 stations minus the smallest) was within 0.1. The regions with relatively large climate index AWC were mainly concentrated within 115°–125 °W. PDO and AMSL showed a coherence of about 0.78 along the eastern Pacific coast of North America, PDO and AMSL showed high correlation, which is similar to the conclusion of Hamlington *et al.* (2014). From the PASC and AWC values, the impact of Niño3.4 on AMSL was greater than SOI, which means that the impact of El Niño on AMSL is greater than that of the southern oscillation. The mean values of PASC and AWC corresponding to Niño 3.4 were the largest among the six climate indexes, which means that ENSO plays a very important role in the change of AMSL in North America.

3.2. Results of MWC analysis

Section 3.1 reports on the significant coherence between the individual climatic indexes and AMSL. Next, we will focus on the relationships between AMSL and combinations of multiple climate indexes.

3.2.1. Niño3.4–PDO

The recent intensification in sea level variability is caused by modulation between the PDO and ENSO, i.e., an El Niño in a positive PDO or a La Niña in a negative PDO phase (Moon *et al.* 2015). However, the changes of PASC and AWC under the action of Niño3.4–PDO are still unknown. Using the MATLAB program provided by Hu & Si (2016), the significant coherence between AMSL and different combinations of multiple climate indexes were obtained. Figure 6 shows the significant coherence results for AMSL and the Niño3.4–PDO combination.

Compared with Niño3.4, under the combined effects of Niño3.4–PDO, the significant coherence area increased significantly, and the average PASC of the 82 stations increased from 14.03 to 49.63%, and the average coherence of the 82 stations also significantly increased from 0.79 to 0.83. This meant that the coherence of Niño3.4–PDO with AMSL was significantly greater than that of Niño3.4 with AMSL. However, the effect of Niño3.4–PDO on AMSL was still localized, and on some time scales there was still no significant coherence.

Compared with Figure 2, where stations 112, 183, 188, 234, 1641, and 430 had almost no significant coherence with only Niño3.4, under the combined effects of Niño3.4–PDO, the coherence and PASC were significantly enhanced. For stations 378, 1269, 1352, 1394, and 2127, the PASC was close to 90% when Niño3.4 and PDO were combined. In general, the time scale of the effect of Niño3.4–PDO on AMSL was longer than that of Niño3.4 or PDO individually on AMSL. The distributions of the PASC and AWC of Niño3.4–PDO for the whole region are shown in Figure 7.

It can be seen that the stations with large PASC values (PASC $\geq$ 85%) were mainly concentrated in the 115 °W–125 °W region, and Niño3.4–PDO had a large impact on the AMSL. In the 70 °W–90 °W region of the east coast of North America, the PASC values were relatively small, and Niño3.4–PDO had a smaller impact on the AMSL. Similar to earlier, the AWC of

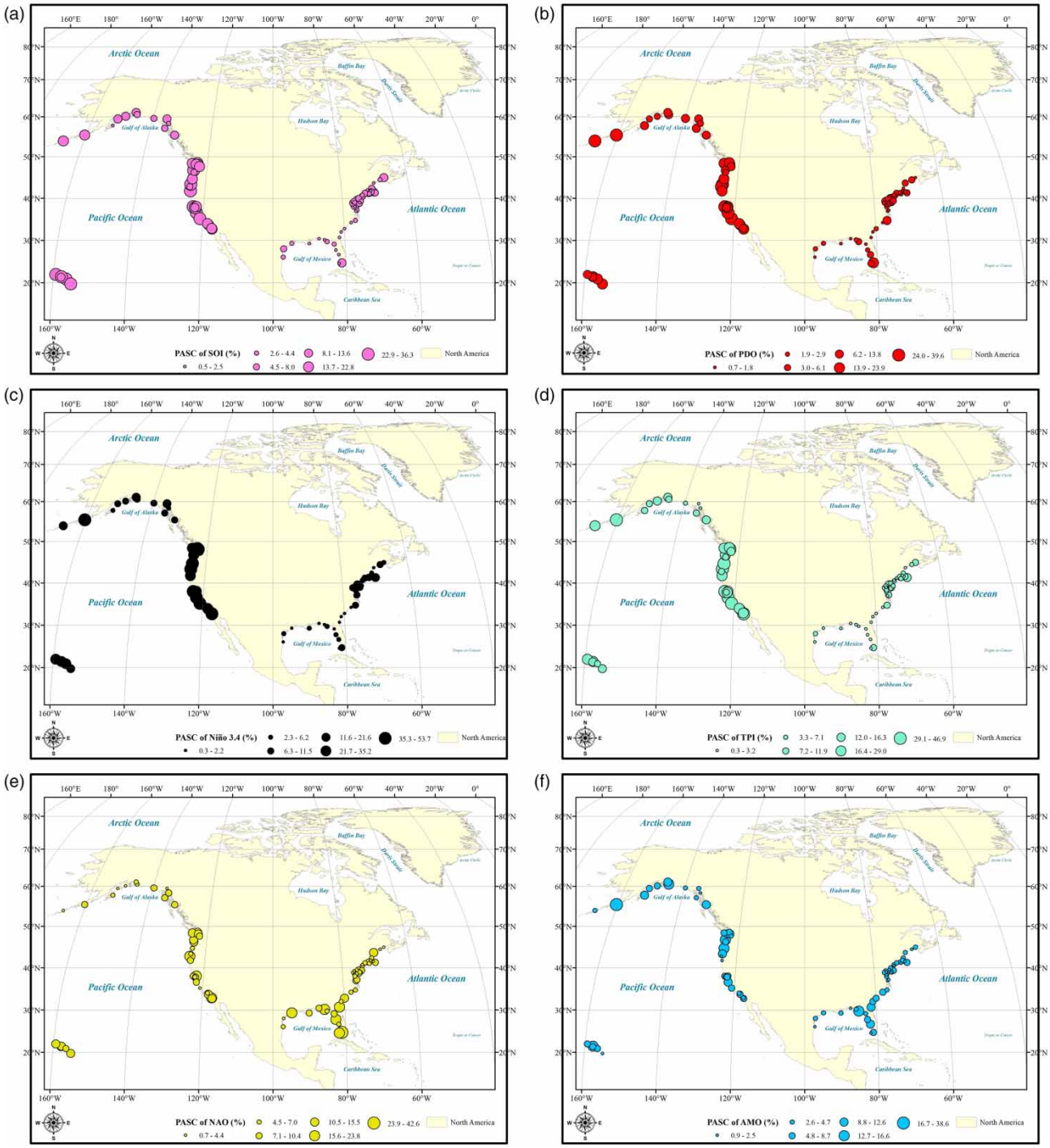

Figure 4 | Distributions of PASC of six climate indexes ((a) SOI, (b) PDO, (c) Niño 3.4, (d) TPI, (e) NAO, and (f) AMO) for AMSL.

different stations did not differ much, with a total range of 0.1, and the distribution of AWC was similar to that of PASC, with relatively larger AWC values within the 120 °W–125 °W region.

Moon *et al.* (2015) studied the response of ENSO–PDO phase relationship changes to sea level changes. He believed that when ENSO and PDO are in phase, the sea level difference is quite large. Our analysis shows that under the action of Niño3.4–PDO, for the east coast of the Pacific Ocean, the high value area of PASC was mainly concentrated in the area

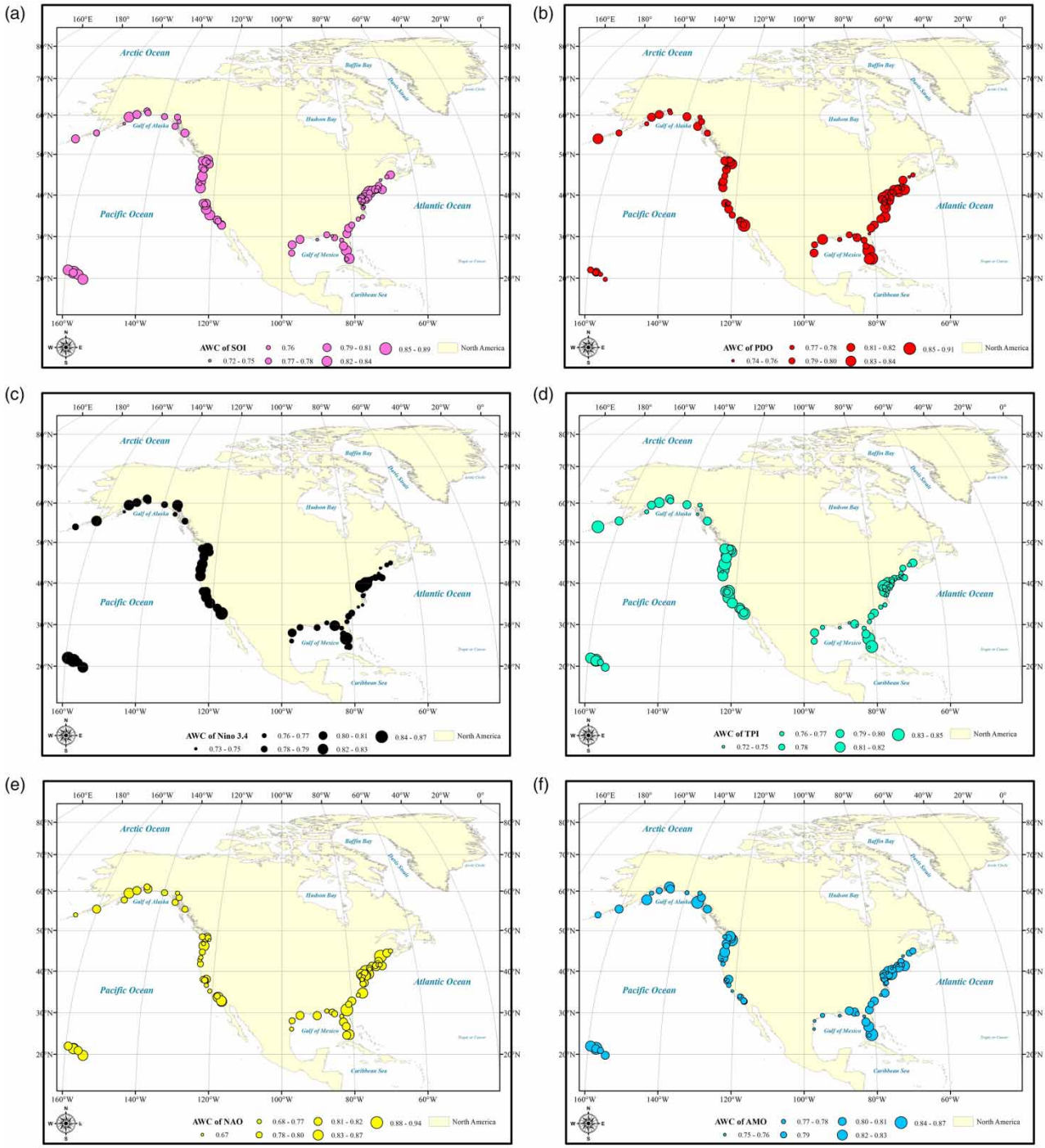

Figure 5 | Distributions of AWC of six climate indexes ((a) SOI, (b) PDO, (c) Niño 3.4, (d) TPI, (e) NAO, and (f) AMO) for AMSL.

of 115–125 °W longitude, and the low value area of PASC was 152–160 °W, this shows that there are regional differences in the influence of Niño3.4–PDO on AMSL. We have a conclusion similar to that of Moon *et al.* (2015) was reached.

Although we did not discuss the modulation effect of PDO on ENSO in different phases, our analysis showed that: The influence of Niño3.4–PDO on AMSL was greater than that of Niño3.4 and PDO on AMSL, because we can see that compared with the effect of Niño3.4 and PDO under the effect of Niño3.4–PDO, PASC and AWC of 82 stations were significantly increased, relative to the effect of Niño3.4 and PDO.

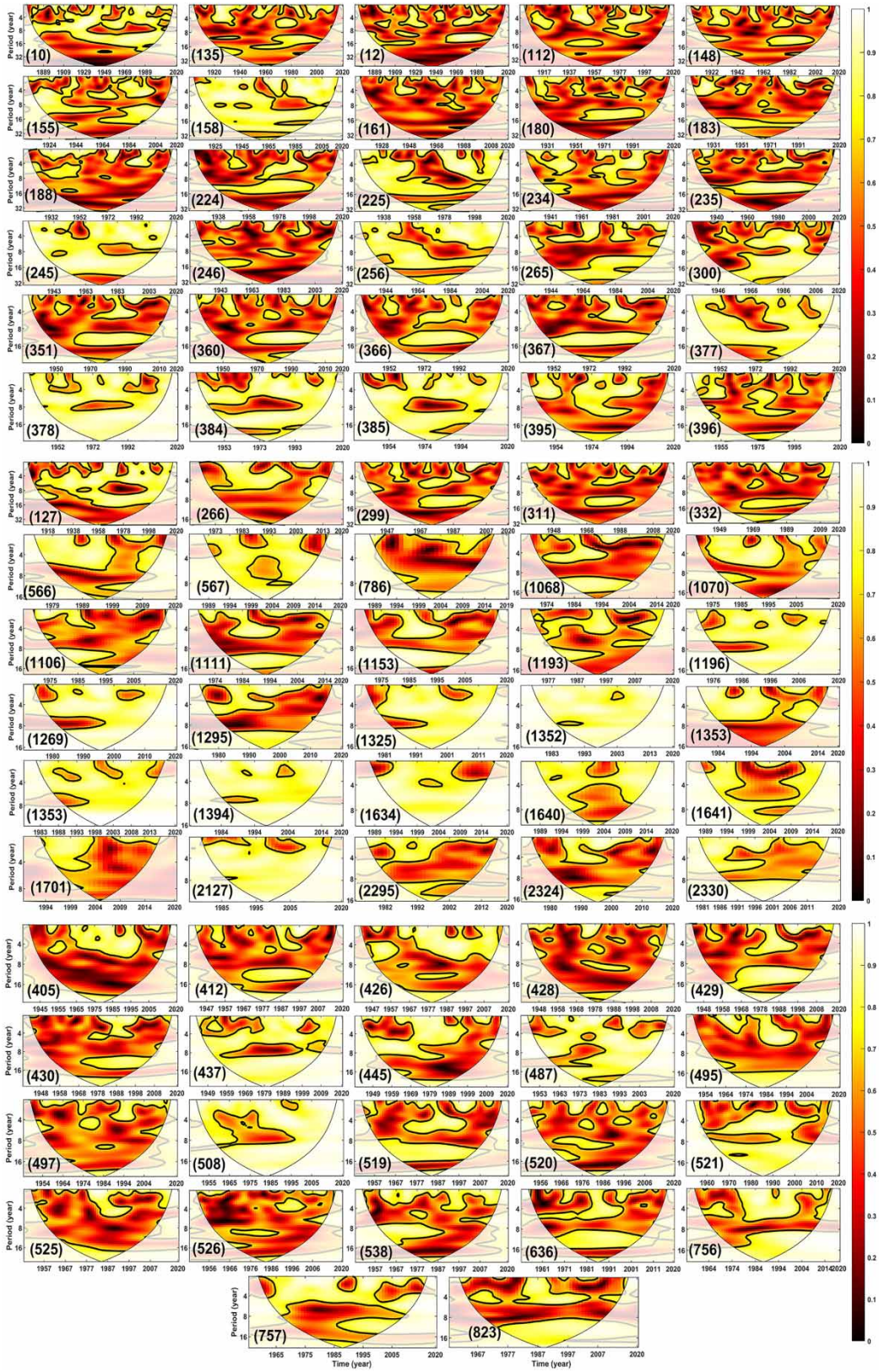

Figure 6 | MWC between AMSL and Niño3.4–PDO. (Thick contours denote 5% significance levels against red noise. The area outside the cone represents the area where edge effects might distort the results.)

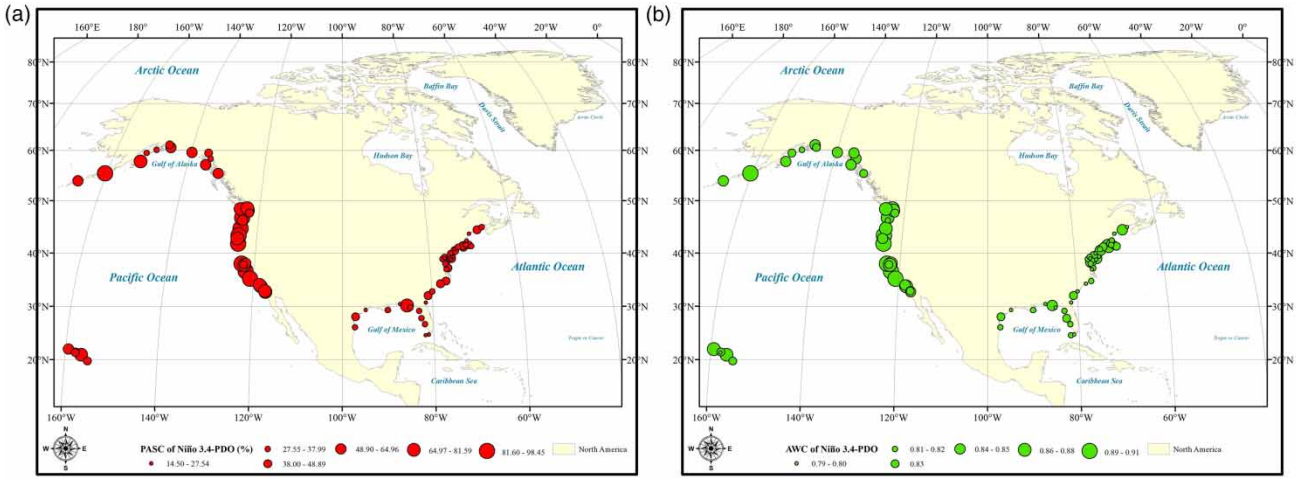

Figure 7 | Distributions of PASC and AWC ((a) PASC and (b) AWC) of Niño3.4–PDO.

3.2.2. Niño3.4–PDO–NAO

Although the relationship between ENSO and NAO is controversial, On the interannual scale, there was a weak inverse correlation between NAO and Niño3.4, which mainly occurred in the years of ENSO events. the two types of ENSO will affect the phase of NAO. The analysis in Section 3.2.1 shows that only using Niño3.4–PDO to reflect the impact of climate on AMSL was not sufficient, because the PASC was not close to 95%. Furthermore, the significant coherence of Niño3.4–PDO did not extend to cover the whole-time domain. Therefore, the significant coherence of AMSL with the Niño3.4–PDO–NAO combination in the whole-time domain was examined, as shown in Figure 8.

As can be seen from Figure 8, compared with Niño3.4 and Niño3.4–PDO, the combined effects of Niño3.4–PDO–NAO had a much higher significant coherence area, and the average PASC and average coherence of the 82 stations increased to 81% and 0.88, respectively. This was significantly greater than the PASC and AWC of Niño3.4 and Niño3.4–PDO, which meant that Niño3.4–PDO–NAO had a stronger influence on AMSL. Furthermore, the time scale of the effect of Niño3.4–PDO–NAO on AMSL was longer than that of Niño3.4–PDO.

For station 1352, PASC reached 100% and the significant coherence covered the entire time domain, which showed that Niño3.4–PDO–NAO was the combination of climate indexes that best matched AMSL changes. Stations 158, 245, 378, 385, 566, 567, 1353, 1394, 1640, and 2127 also had, in addition to extremely high significant coherence areas, PASC values greater than 90% and average coherences of more than 0.9. Compared with the PASC values under Niño3.4–PDO, the PASC of 10 stations increased by more than 50% under Niño3.4–PDO–NAO, and the PASC of stations 112, 161, 180, 183, 188, 234, 246, 428, 786, and 1701 (with longitudes ranging from about 75 °W–100 °W) increased by 66, 62, 51, 50, 56, 54, 59, 51, 62, and 57%, respectively. The distributions of PASC and AWC between AMSL and Niño3.4–PDO–NAO are shown in Figure 9.

It can be seen that the stations with large PASC values (PASC $\geq$ 95%) were mainly concentrated in the 120 °W–125 °W region and that Niño3.4–PDO–NAO had a large impact on the AMSL. In the 70 °W–90 °W region of the east coast of North America, the PASC values were relatively small, and Niño3.4–PDO–NAO had only a small impact on the change of AMSL. The AWC values of the different stations did not differ much, basically ranging within 0.1. The distribution of AWC was similar to that of PASC, with relatively large AWC values between 120 °W and 125 °W and relatively small AWC values between 70 °W and 90 °W. This was consistent with the significant coherence analysis of Niño3.4–PDO and AMSL.

3.2.3. Niño3.4–PDO–NAO–AMO

In the analysis in Section 3.2.2 we found that, despite the combined effect of Niño3.4–PDO–NAO, the PASC of most stations did not reach 100%. This meant that other climate indexes need to be added to further increase PASC. According to the study by Hu *et al.* (2017), when adding variables, any variable that leads to an increase of at least 5% in PASC is considered important. Following this threshold, we added AMO to discuss how the PASC of AMSL changed under the combined effect of

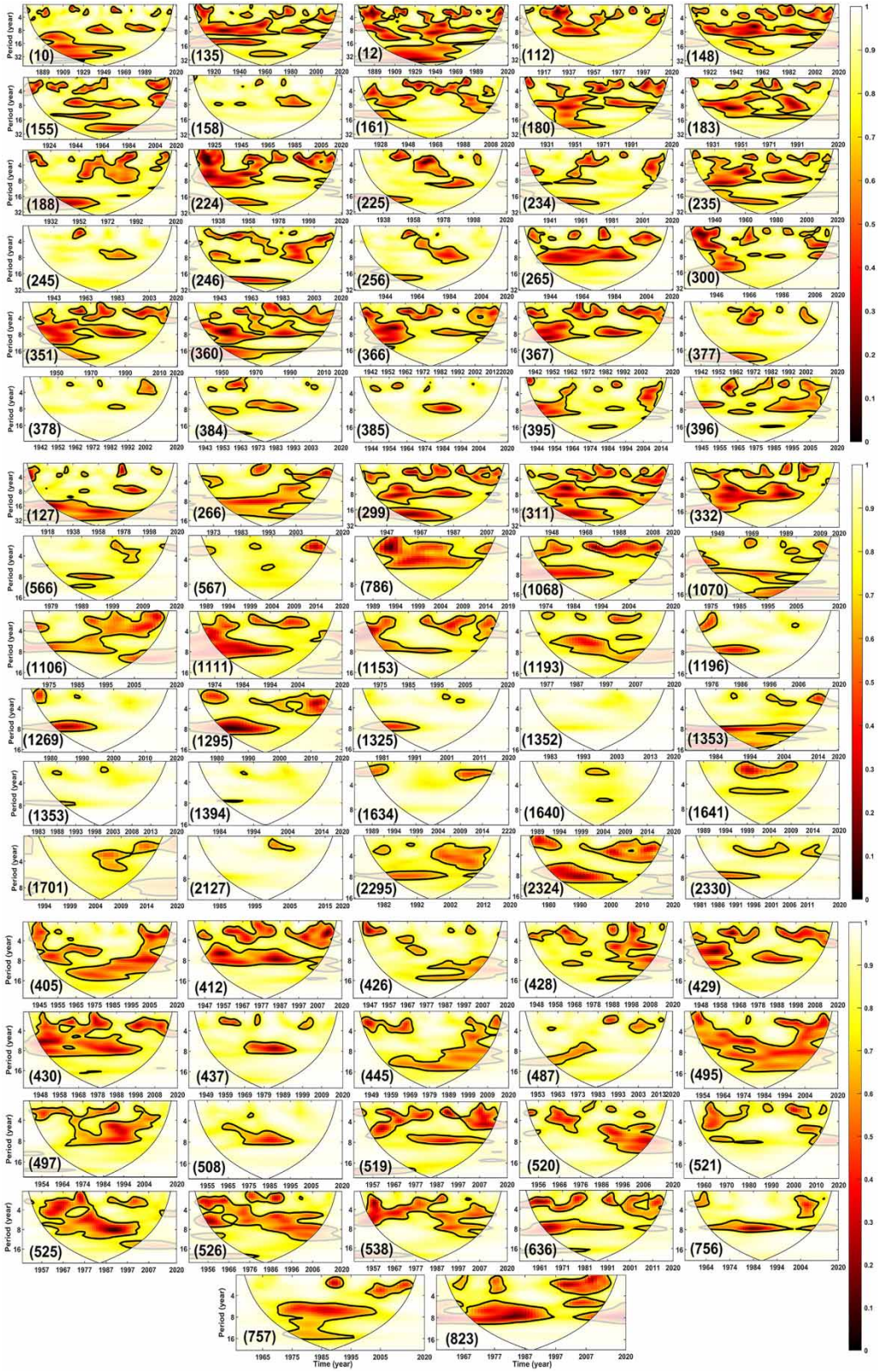

Figure 8 | MWC between AMSL and Niño3.4–PDO–NAO. (Thick contours denote 5% significance levels against red noise. The area outside the cone represents the area where edge effects might distort the results.) Please refer to the online version of this paper to see this figure in colour: http://dx.doi.org/10.2166/wcc.2022.180.

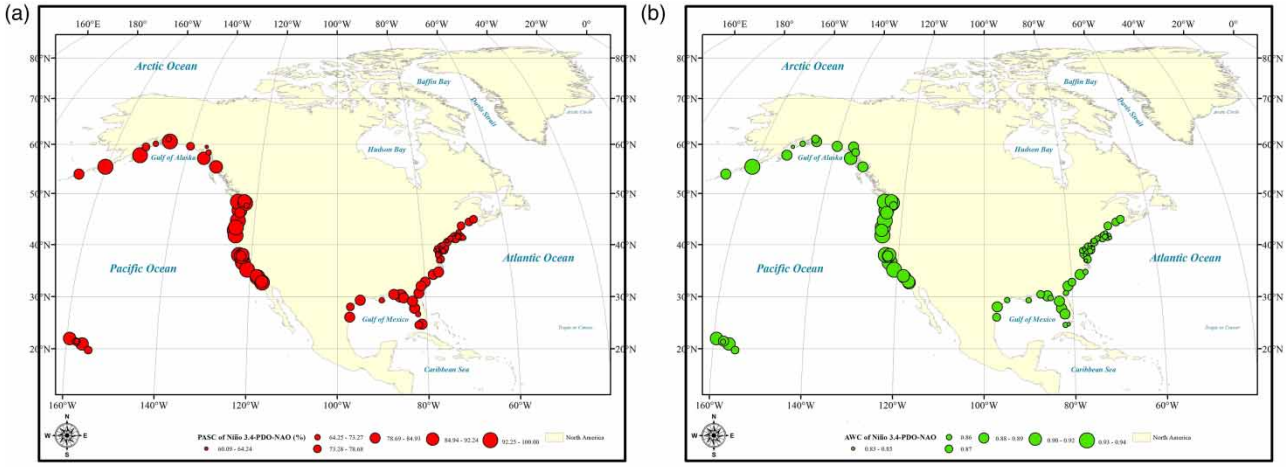

Figure 9 | Distributions of PASC and AWC ((a) PASC and (b) AWC) of Niño3.4–PDO–NAO.

Niño3.4–PDO–NAO–AMO. The significant coherence between Niño3.4–PDO–NAO–AMO and AMSL is shown in Figure 10.

Compared with the PASC of Niño3.4–PDO–NAO, the PASC between Niño3.4–PDO–NAO–AMO and AMSL increased significantly, which meant that the addition of AMO increased the explanatory power for the changes in AMSL. The PASC of stations 1352, 1354, 1394, 1634, 1640, 2127, and 2330 reached 100%, which meant that Niño3.4–PDO–NAO–AMO was sufficient to explain the changes in AMSL of these stations. The distributions of PASC and AWC for AMSL and Niño3.4–PDO–NAO–AMO are shown in Figure 11.

We found that the PASC values were higher in the 50 °N–60 °N and 150 °W–180 °W regions, and that the PASC values were about 98%. The PASC values were also higher in the 115 °W–125 °W and 30 °N–50 °N regions. In these regions, Niño3.4–PDO–NAO–AMO had the greatest impact on AMSL. Within 120 °W–125 °W, AWC was the largest and at 70 °W–90 °W, AWC was the smallest.

Under the combined effects of Niño3.4–PDO–NAO–AMO, the PASC ranged within 85.35–100%, and the range of the AWC was 0.89–0.98, which were significantly greater than the PASC and AWC under Niño3.4, Niño3.4–PDO, and Niño3.4–PDO–NAO. This meant that Niño3.4–PDO–NAO–AMO had a greater overall impact on AMSL than the other indexes and index combinations.

3.2.4. Niño3.4–PDO–NAO–AMO–TPI

In the analysis presented in Section 3.2.3, the PASC values of some stations were still lower than 95%, which meant that adding another climate index may further improve the PASC. Therefore, in this section we discuss the PASC under the combined effect of Niño3.4–PDO–NAO–AMO–TPI, shown in Figure 12.

It can be seen that there was significant coherence for the entire time domain for most stations. The effect of Niño3.4–PDO–NAO–AMO–TPI on AMSL was the whole-time domain, which meant Niño3.4–PDO–NAO–AMO–TPI was sufficient to explain the changes in AMSL. However, nine of the 82 stations (135, 148, 180, 224, 300, 786, and 405) had PASC values between 94 and 95%, i.e., they were lower under Niño3.4–PDO–NAO–AMO–TPI. This meant that, in addition to Niño3.4, PDO, NAO, AMO, and TPI, the changes in AMSL at these stations may be influenced by other climate indexes, and that PASC may or may not continue to increase with additional indexes. Despite this, under the combined effects of Niño3.4–PDO–NAO–AMO–TPI, all 82 stations had sufficiently large PASC values and their significant coherence basically covered the entire time domain. Based on the explanatory power of this combination of indexes, the influences of other climate indexes on the significant coherence of AMSL were not considered in detail. The PASC and AWC distributions of Niño3.4–PDO–NAO–AMO–TPI and AMSL are shown in Figure 13.

Under the combined effects of Niño3.4–PDO–NAO–AMO–TPI, both the PASC and AWC had high values for all stations, with PASC ranging from 95.87 to 100% and AWC ranging from 0.938 to 0.991, which were significantly greater than the PASC and AWC under Niño3.4–PDO–NAO–TPI.

Figure 10 | MWC between AMSL and Niño3.4–PDO–NAO–AMO. (Thick contours denote 5% significance levels against red noise. The area outside the cone represents the area where edge effects might distort the results.) Please refer to the online version of this paper to see this figure in colour: http://dx.doi.org/10.2166/wcc.2022.180.

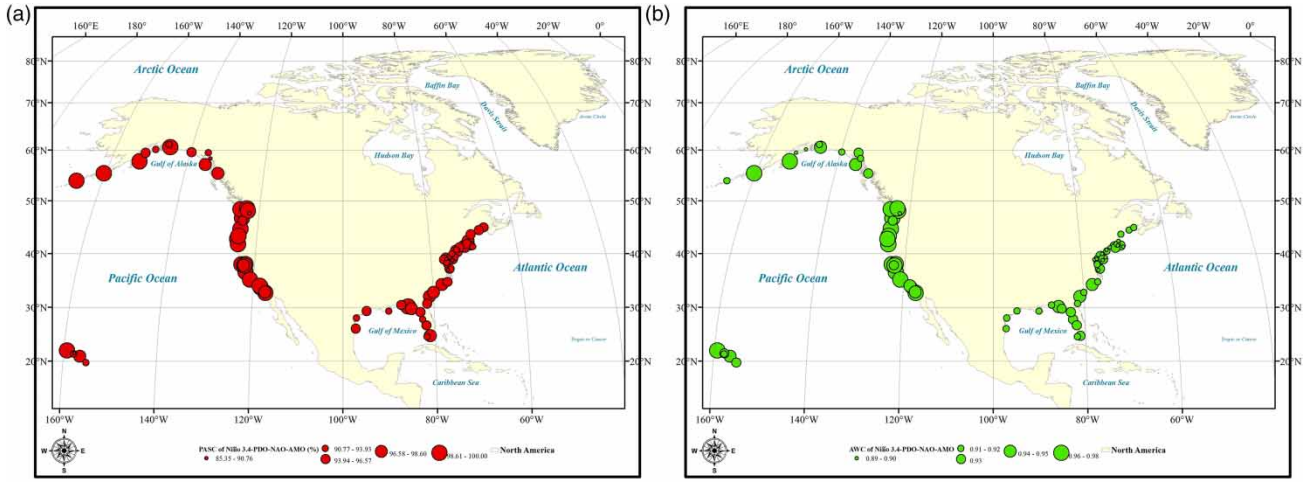

Figure 11 | Distributions of PASC and AWC ((a) PASC and (b) AWC) of Niño3.4–PDO–NAO–AMO.

According to Hu & Si (2016), when the addition of a climate index leads to an increase in PASC of more than 5%, the climate index is important. Therefore, with Niño3.4–PDO–NAO–AMO–TPI already returning minimum PASC values of 95.37%, any further increase of 5% in PASC is impossible. With such a high explanatory power already being achieved, there is no need to add additional climate indexes to explain the changes in AMSL.

4. DISCUSSION

4.1. Which four climate indexes are the best combination of the four climate indexes?

The analysis in Section 3.2 showed that the PASC values corresponding to Niño3.4–PDO and Niño3.4–PDO–NAO were not optimal. Their average PASC values were 49.63 and 81.11%, respectively. By adding additional important climate indexes, the average PASC can be increased by more than 5%. Therefore, Niño3.4–PDO and Niño3.4–PDO–NAO were not the optimal combinations because two or three climate indexes have insufficient explanatory power, so the other two or three climate index combinations were not considered. To determine which four climate indexes are the best combination of the four climate indexes, we compared the PASC of Niño3.4–PDO–NAO–AMO to PDO–NAO–AMO–SOI and PDO–NAO–AMO–TPI, as shown in Figure 14.

We found that the PASC of Niño3.4–PDO–NAO–AMO was not very different from PDO–NAO–AMO–TPI or PDO–NAO–AMO–SOI, and the PASC difference at most stations was within plus or minus 3%. The PASC differences between Niño3.4–PDO–NAO–AMO and PDO–NAO–AMO–TPI were greater than or equal to 0 at 59% of stations, and stations 10, 127, 155, 180, and 1068 had the largest PASC differences, at 11.04, −6.91, 14.62, 31.95, and 28.48%, respectively. The PASC differences between of Niño3.4–PDO–NAO–AMO and PDO–NAO–AMO–SOI were greater than or equal to 0 at 40% of the stations, and those of stations 127 and 1068 were largest, −6.17 and 28.48%, respectively.

Furthermore, the average PASC values of Niño3.4–PDO–NAO–AMO, PDO–NAO–AMO–TPI and PDO–NAO–AMO–SOI were 96.00, 95.06, and 95.83%, respectively. The average PASC values of Niño3.4–PDO–NAO–AMO and PDO–NAO–AMO–TPI had a large difference (0.94%), while those of Niño3.4–PDO–NAO–AMO and PDO–NAO–AMO–SOI had a small difference (0.17%). By comparing the PASC of Niño3.4, TPI, and SOI, we found that the PASC of Niño3.4 was higher than those of TPI and SOI at 61 and 57% of the stations, respectively. In addition, the average PASC of Niño3.4 among the 82 stations was 14.03%, higher than the average PASC of TPI (12.92%) and SOI (10.86%), but the differences in AWC were small.

After examining the PASC of single climate indexes and the average PASC values of Niño3.4–PDO–NAO–AMO, PDO–NAO–AMO–TPI, and PDO–NAO–AMO–SOI, we recommend Niño3.4–PDO–NAO–AMO as the optimal combination of four climate indexes.

Figure 12 | The PASC and AWC of Niño3.4–PDO–NAO–AMO–TPI. (Thick contours denote 5% significance levels against red noise. The area outside the cone represents the area where edge effects might distort the results.) Please refer to the online version of this paper to see this figure in colour: http://dx.doi.org/10.2166/wcc.2022.180.

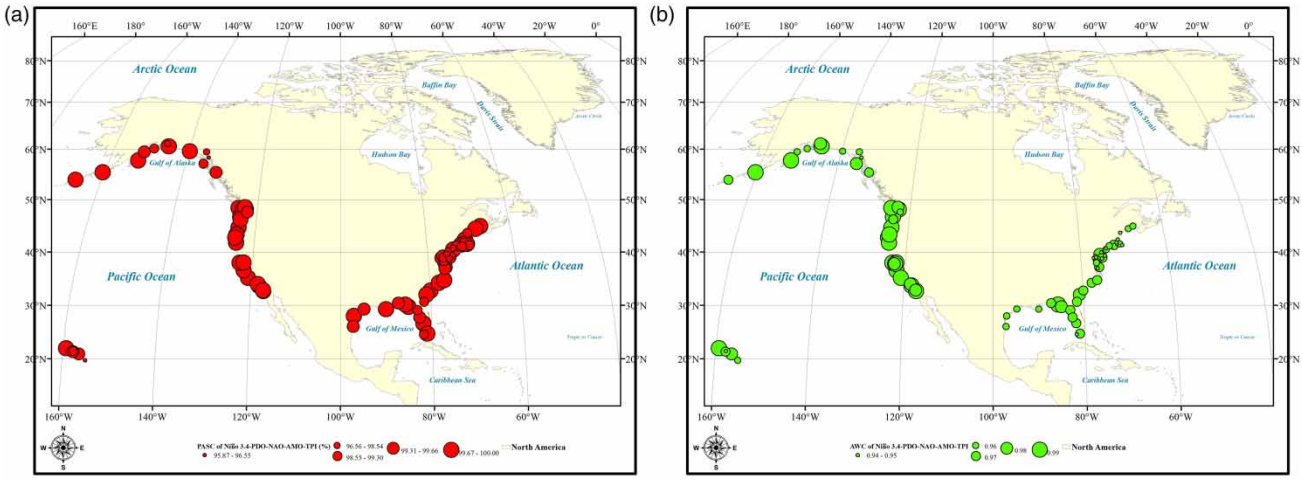

Figure 13 | Distributions of PASC and AWC ((a) PASC and (b) AWC) of Niño3.4–PDO–NAO–AMO–TPI and AMSL.

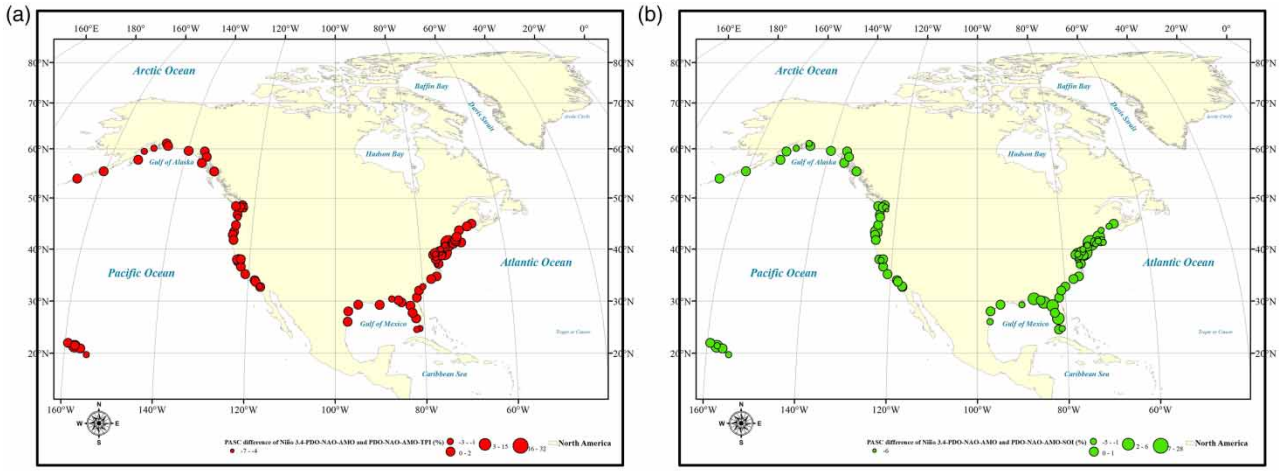

Figure 14 | Difference between the PASC values of Niño3.4–PDO–NAO–AMO and those of PDO–NAO–AMO–TPI (a) and PDO–NAO–AMO–SOI (b). (*Note:* The scale of the color bar is more positive, indicating that the PASC of Niño3.4–PDO–NAO–AMO was generally greater than those of PDO–NAO–AMO–TPI or PDO–NAO–AMO–SOI. If the scale of the color bar was negative, it would indicate that the PASC of Niño3.4–PDO–NAO–AMO was smaller than those of PDO–NAO–AMO–TPI or PDO–NAO–AMO–SOI.) Please refer to the online version of this paper to see this figure in colour: http://dx.doi.org/10.2166/wcc.2022.180.

4.2. How many climate indexes are adequate to explain AMSL?

Previous studies (Hamlington *et al.* 2015; Moon *et al.* 2015) usually only include a single climate variable, such as ENSO and PDO, to explain sea level change, which may be inadequate in the interpretation of sea level change, because scale dependence and local information were previously ignored (Hu *et al.* 2017).

Sections 3.1 and 3.2 describe the impacts of single climate indexes and multiple climate indexes on AMSL, a single climate index is not sufficient to explain the change of AMSL. Therefore, it is necessary to add additional climate indexes to reflect the change of AMSL. However, simply increasing the number of climate indexes does not guarantee they will be sufficient to explain the change in AMSL. This is because the increases of PASC and AWC may not be obvious (Under Niño3.4–PDO–NAO–AMP–TPI, PASC was above 95% and AWC was above 0.95). Therefore, we integrated the PASC and AWC values at each station based on the research of Hu & Si (2016) and finally determined the best climate index combination to explain AMSL at 82 stations in North America, as shown in Figure 15.

It can be seen that the Niño3.4–PDO–NAO combination was best within 122 °W–126 °W, while the best climate index combinations within 150 °W–180 °W and 50 °N–60 °N was Niño3.4–PDO–NAO–AMO. In addition, the region within

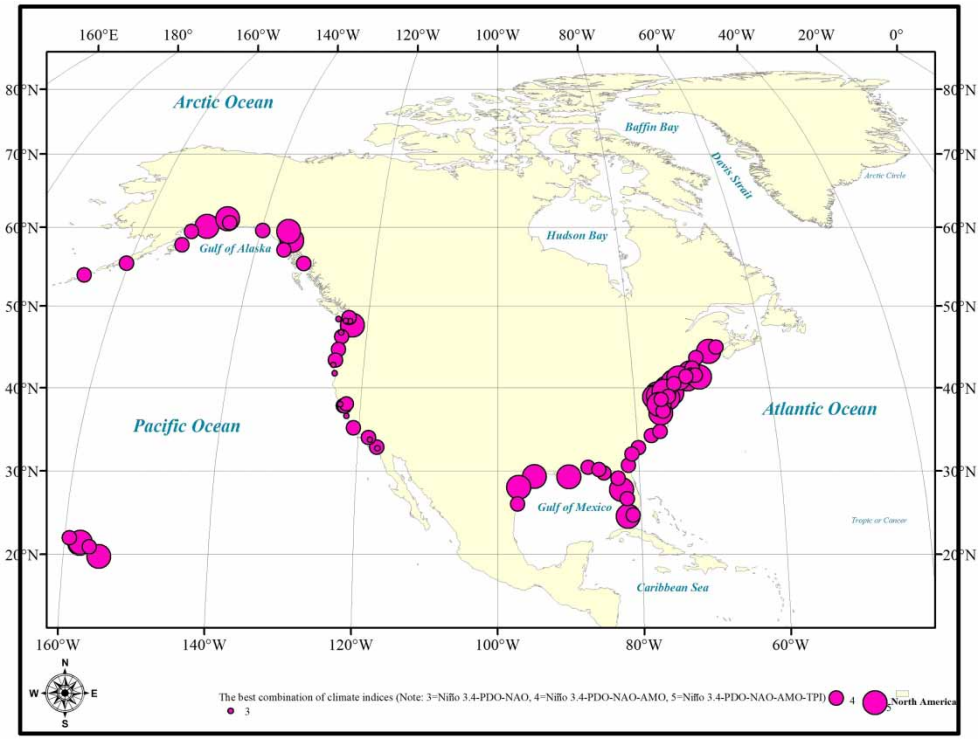

Figure 15 | Optimized climate index combinations for AMSL at 82 stations.

65 °W–90 °W corresponded to the Niño3.4–PDO–NAO–AMO combination. The Niño3.4–PDO–NAO–AMP–TPI combination was mainly best within 67 °W–76 °W and 90 °W–98 °W.

In short, to reflect the changes in AMSL in most regions of North America, at least three climate indexes (Niño3.4–PDO–NAO; 122 °W–126 °W) are required, but sometimes four (Niño3.4–PDO–NAO–AMO) or five (Niño3.4–PDO–NAO–AMO–TPI) climate indexes are best. Although only six climate indexes were examined in this study, they were selected because of their close relationship to AMSL, so the impact of other climate indexes on AMSL were not discussed in depth. Other climate indexes may indirectly affect PDO or ENSO events. However, under various climate index combinations, especially the Niño3.4–PDO–NAO–AMO–TPI combination, AWC and PASC were sufficiently large (see Figure 13). The PASC of Niño3.4–PDO–NAO and Niño3.4–PDO–NAO–AMO were also large enough at some stations, and the PASC values of Niño3.4–PDO–NAO–AMO–TPI were basically large enough across the whole-time domain, which meant that it is sufficient to explain the changes in AMSL on various time scales.

4.3. Future prospects

Although MWC cannot reflect the modulation effect of a single climate index on ENSO, nor can it reflect the modulation effect of multiple climate indexes on ENSO, revealing the modulation effect of multiple climate indexes on ENSO (the effect of different phases on ENSO) is an extremely complex and challenging task. The AWC and PASC values of MWC provide the possibility to understand the combined effects of multiple climate indexes on AMSL and ENSO. In addition, wavelet coherence and multivariable wavelet coherence provide the possibility to understand the dominant factors and complex mechanism of sea level change. PASC value and AWC value can be used to screen out the best influencing factors. However, the traditional principal component analysis cannot reflect the influence of dependent variables on independent variables in time scale. In addition, complex factors, such as the rotation of the Earth, affect atmospheric circulation, which in turn influences sea level changes, although these effects are not considered in this paper. The research conducted in this paper also provides the possibility to understand the impact of earth rotation on sea level, which can be qualitatively judged by PASC and AWC values.

In the future, we will further study the influence of multiple climate indexes on AMSL at different phases and the mechanisms of sea level change.

5. CONCLUSIONS

Using wavelet coherence and MWC to study the time scale relationship between the AMSL and climate indicators at 82 stations in North America, the following conclusions can be drawn: Among the six climate indexes, Niño 3.4 has the strongest significant coherence with AMSL. However, the time scale of the effect of a single climate index on AMSL is localized. Therefore, the joint action of multiple climate indexes was needed to improve the global explanatory power of climate indexes on the time scales of AMSL. Three to five climate indexes (Niño3.4–PDO–NAO, Niño3.4–PDO–NAO–AMO, Niño3.4–PDO–NAO–AMO–TPI) were sufficient to reflect the change of AMSL, depending on the region.

The MWC was used to identify the best combination of independent variables by calculating the PASC and AWC of independent variables. The larger the PASC and AWC, the more important the independent variable, which also provides a new method for screening the best predictor of sea level. This new method provides an effective means to resolve the complex spatial and temporal variability of multiple control factors over multiple temporal scales. The methods used in this study are universal and can serve as a reference for screening the best independent variables for dependent variables in other fields.

It must be noted that we only discussed the impacts of Niño3.4, PDO, NAO, AMO, SOI, and TPI on AMSL, and did not discuss the impacts of other climate indexes or factors (glacier melting, population growth) on AMSL. In future studies, we will further explore the influence of these factors on AMSL in North America.

ACKNOWLEDGEMENTS

Data supporting all figures and tables are freely available upon request from the corresponding author. The codes for calculating wavelet coherence are available from Grinsted *et al.* (2004) and can be downloaded from the website (http://grinsted.github.io/wavelet-coherence/). The codes for calculating MWC are available from Hu & Si (2016) and can be downloaded from the website (http://www.hydrol-earth-syst-sci.net/20/3183/2016/hess-20-3183-2016-supplement.pdf). This research was financially supported by the National Natural Science Foundation of China (Grant Nos U1911204 and 51861125203), The National Key R&D Program of China (2017YFC0405900), and the Project for Creative Research from the Guangdong Water Resources Department (Grant No. 2018, 2020).

DECLARATION OF COMPETING INTEREST

The authors declare that they have no known competing financial interests or personal relationships that could have appeared to influence the work reported in this paper.

DATA AVAILABILITY STATEMENT

All relevant data are included in the paper or its Supplementary Information.

CONFLICT OF INTEREST

The authors declare there is no conflict.

REFERENCES

Chafik, L., Nilsen, J. E. Ø., Dangendorf, S., Reverdin, G. & Frederikse, T. 2019 North Atlantic Ocean circulation and decadal sea level change during the altimetry era. *Scientific Reports* **9**, 1–9. https://doi.org/10.1038/s41598-018-37603-6.

Cheng, Q., Zhong, F. & Wang, P. 2021 Baseflow dynamics and multivariate analysis using bivariate and multiple wavelet coherence in an alpine endorheic river basin (Northwest China). *Science of The Total Environment* **772**, 1–20. https://doi.org/10.1016/j.scitotenv.2021.145013.

Durocher, M., Lee, T. S., Ouarda, T. & Chebana, F. 2016 Hybrid signal detection approach for hydro-meteorological variables combining EMD and cross-wavelet analysis. *International Journal of Climatology* **36** (4). https://doi.org/10.1002/joc.4444.

Grinsted, A., Moore, J. C. & Jevrejeva, S. 2004 Application of the cross wavelet transform and wavelet coherence to geophysical time series. *Nonlinear Processes in Geophysics* **11**, 561–566. https://doi.org/10.5194/npg-11-561-2004.

Gu, X., Sun, H. G., Zhang, Y., Yu, Z. & Zhu, J. 2021 Multiple wavelet coherence to evaluate local multivariate relationships in a groundwater system. *Groundwater* **59** (3), 443–452. https://doi.org/10.1111/gwat.13068.

Haddad, M., Taibi, H. & Si, M. 2013 On the recent global mean sea level changes: trend extraction and EI Niño's impact. *Comptes Rendus Geoscience* **345**, 167–175. http://dx.doi.org/10.1016/j.crte.2013.03.002.

Hamlington, B. D. & Thompson, P. R. 2015 Considerations for estimating the 20th century trend in global mean sea level. *Geophysical Research Letters* **42**, 4102–4109. https://doi.org/10.1002/2015GL064177.

Hamlington, B. D., Strassburg, M. W., Leben, R. R., Han, W., Nerem, R. S. & Kim, K. Y. 2014 Uncovering an anthropogenic sea-level rise signal in the Pacific Ocean. *Nature Climate Change* **4**, 782–785. https://doi.org/10.1038/nclimate2307.

Hamlington, B. D., Leben, R. R., Kim, K. Y., Nerem, R. S., Atkinson, L. P. & Thompson, P. R. 2015 The effect of the El Niño-Southern Oscillation on U.S. regional and coastal sea level. *Journal of Geophysical-Oceans* **120**, 3970–3986. https://doi.org/10.1002/2014JC010602.

Hannah, J. & Bell, R. G. 2012 Regional sea level trends in New Zealand. *Journal of Geophysical Research Oceans* **117**, 1–7. https://doi.org/10.1029/2011JC007591.

Henley, B. J., Gergis, J., Karoly, D. J., Power, S. B., Kennedy, J. & Folland, C. K. 2015 A tripole index for the interdecadal pacific oscillation. *Climate Dynamics* **45**, 3077–3090. http://dx.doi.org/10.1007/s00382-015-2525-1.

Holgate, S. J., Matthews, A., Woodworth, P. L., Rickards, L. J., Tamisiea, M. E., Bradshaw, E., Foden, P. R., Gordon, K. M., Jevrejeva, S. & Pugh, J. 2013 New data systems and products at the permanent service for mean sea level. *Journal of Coastal Research.* **29** (3), 493–504. https://doi.org/10.2112/JCOASTRES-D-12-00175.1.

Hu, W. & Si, B. C. 2016 Technical note: multiple wavelet coherence for untangling scale-specific and localized multivariate relationships in geosciences. *Hydrology & Earth System Sciences* **20**, 3183–3191. https://doi.org/10.5194/hess-20-3183-2016.

Hu, W., Si, B. C., Biswas, A. & Chau, H. W. 2017 Temporally stable patterns but seasonal dependent controls of soil water content: evidence from wavelet analyses. *Hydrological Processes* **31** (21), 3697–3707. https://doi.org/10.1002/hyp.11289.

Hurrell, J. W., Kushnir, Y., Ottersen, G. & Visbeck, M. 2003 *An Overview of the North Atlantic Oscillation*. https://doi.org/10.1029/134GM01. American Geophysical Union.

Jevrejeva, S., Moore, J. C. & Grinsted, A. 2003 Influence of the Arctic Oscillation and El Niño-Southern Oscillation (ENSO) on ice conditions in the Baltic Sea: the wavelet approach. *Journal of Geophysical Research* **108**, 4677. https://doi.org/10.1029/2003JD003417.

Jevrejeva, S., Grinsted, A., Moore, J. C. & Holgate, S. 2006 Nonlinear trends and multiyear cycles in sea level records. *Journal of Geophysical Research* **111**, 1–11. https://doi.org/10.1029/2005JC003229.

Kirikkaleli, D. & Sowah, J. K. 2021 Time-frequency dependency of temperature and sea level: a global perspective. *Environment Science Pollution Research* **28**, 58787–58798. https://doi.org/10.1007/s11356-021-14846-x.

Little, C. M., Piecuch, C. G. & Ponte, R. M. 2021 North American east coast sea level exhibits high power and spatiotemporal complexity on decadal timescales. *Geophysical Research Letters* **48** (15), 1–10. https://doi.org/10.1029/2021GL093675.

Liu, X. Y., Liu, Y. G., Guo, L., Rong, Z. R., Gu, Y. Z. & Liu, Y. H. 2010 Interannual changes of sea level in the two regions of East China Sea and different responses to ENSO. *Global & Planetary Change* **55** (4), 257–272. https://doi.org/10.1016/j.gloplacha.2010.04.009.

Mantua, N. J., Hare, S. R., Zhang, Y., Wallace, J. M. & Francis, R. C. 1997 A pacific interdecadal climate oscillation with impacts on salmon production. *Bulletin of the American Meteorological Society* **78** (6), 1069–1079. https://doi.org/10.1175/1520-0477(1997)078<1069:APICOW>2.0.CO;2.

Medvedev, I. & Kulikov, E. 2019 Low-frequency Baltic sea level spectrum. *Frontiers in Earth Science* **7** (284), 1–14. https://doi.org/10.3389/feart.2019.00284.

Moon, J. H., Song, Y. T. & Lee, H. 2015 PDO and ENSO modulations intensified decadal sea level variability in the tropical Pacific. *Journal of Geophysical-Oceans* **120**, 8229–8237. https://doi.org/10.1002/2015JC011139.

Nalley, D., Adamowski, J., Biswas, A., Gharabaghi, B. & Hu, W. 2019 A multiscale and multivariate analysis of precipitation and streamflow variability in relation to ENSO, NAO and PDO. *Journal of Hydrology* **574**, 288–307. https://doi.org/10.1016/j.jhydrol.2019.04.024.

Nourani, V., Ghasemzade, M., Mehr, A. D. & Sharghi, E. 2019 Investigating the effect of hydroclimatological variables on urmia lake water level using wavelet coherence measure. *Journal of Water and Climate Change* **10** (1), 13–29. https://doi.org/10.2166/wcc.2018.261.

Permanent Service for Mean Sea Level (PSMSL) 2021 *Tide Gauge Data*. Available from: http://www.psmsl.org/data/obtaining/ (accessed 09 August 2021).

Piecuch, C. G., Dangendorf, S., Gawarkiewicz, G. G., Little, C. M., Rui, M. P. & Yang, J. 2019 How is new England coastal sea level related to the Atlantic meridional overturning circulation at 26 °N? *Geophysical Research Letters* **46** (10), 1–10. https://doi.org/10.1029/2019GL083073.

Rohith, B., Paul, A., Durand, F., Testut, L., Prerna, S., Afroosa, M., Ramakrishna, S. S. V. S. & Shenoi, S. S. C. 2019 Basin-wide sea level coherency in the tropical Indian Ocean driven by Madden–Julian Oscillation. *Nature Communication* **10**, 1–9. https://doi.org/10.1038/s41467-019-09243-5.

Song, X. M., Zhang, C. H., Zhang, J. Y., Zou, X. J., Mo, Y. C. & Tian, Y. M. 2020 Potential linkages of precipitation extremes in Beijing-Tianjin-Hebei region, China, with large-scale climate patterns using wavelet-based approaches. *Theoretical and Applied Climatology* **141**, 1251–1269. https://doi.org/10.1007/s00704-020-03247-8.

Tang, J., Li, Q. Y. & Chen, J. 2018 Summertime runoff variations and their connections with Asian summer monsoons in the Yangtze river basin. *Journal of Water and Climate Change* **9** (1), 89–100. https://doi.org/10.2166/wcc.2017.142.

Tiwari, V. M., Cabanes, C., Dominh, K. & Cazenave, A. 2004 Correlation of interannual sea level variations in the Indian ocean from topex/poseidon altimetry, temperature data and tide gauges with ENSO. *Global & Planetary Change* **43**, 183–196. https://doi.org/10.1016/j.gloplacha.2004.08.001.

Torrence, C. G. & Compo, G. P. 1998 A practical guide to wavelet analysis. *Bulletin of the American Meteorological Society* **79** (1), 61–78. https://doi.org/10.1175/1520-0477(1998)079<0061:APGTWA>2.0.CO;2.

Torrence, C. & Webster, P. 1999 Interdecadal changes in the ESNO-monsoon system. *Journal of Climate* **12**, 2679–2690.

Volkov, D. L., Baringer, M. O., Smeed, D., Johns, W. E. & Landerer, F. W. 2019 Teleconnection between the atlantic meridional overturning circulation and sea level in the Mediterranean Sea. *Journal of Climate* **32**, 935–955. https://doi.org/10.1175/JCLI-D-18-0474.1.

Wang, H., Pan, Y. & Chen, Y. 2018 Impacts of regional climate and teleconnection on hydrological change in the bosten lake basin, arid region of northwestern China. *Journal of Water and Climate Change* **9** (1), 74–88. https://doi.org/10.2166/wcc.2017.142.

Wenzel, M. & Schröter, J. 2014 Global and regional sea level change during the 20th century. *Journal of Geophysical Research-Oceans* **119**, 7493–7508. https://doi.org/10.1002/2014JC009900.

Xi, H., Zhang, Z. & Lu, Y. 2020 A quasi-decadal oscillation of sea-level variation in the South China Sea. *Journal of Coastal Research* **36** (2), 228–237. https://doi.org/10.2112/JCOASTRES-D-19-00078.1.

Yu, H. L. & Lin, Y. C. 2015 Analysis of space–time non-stationary patterns of rainfall–groundwater interactions by integrating empirical orthogonal function and cross wavelet transform methods. *Journal of Hydrology* **525**, 585–597. http://dx.doi.org/10.1016/j.jhydrol.2015.03.057.

Zhang, X. & Church, J. A. 2012 Sea level trends, interannual and decadal variability in the Pacific Ocean. Sea level trends, interannual and decadal variability in the Pacific Ocean. *Geophysical Research Letters* **39** (21), 1–8. https://doi.org/10.1029/2012GL053240.

First received 22 May 2022; accepted in revised form 30 August 2022. Available online 8 September 2022